Motion Compensated LIDAR Scanning for Small Robots

Dingkang Wang[1], Yuyang Chen[2], Lenworth Thomas[3], Huikai Xie[4], Karthik Dantu[2], Sanjeev J. Koppal[1]

***Abstract*— Microrobots experience significant egomotion due to high-frequency actuation and their susceptibility to external forces such as wind. This affects onboard sensors and any control that depends on that sensing. Egomotion compensation in software is challenging because of the delay as well as the computing and energy resources required. We present a novel microelectromechanical (MEMS) mirror LiDAR system for small robots where the motion of the robot is compensated, in hardware, by an on-board IMU that drives the MEMS mirror. Additionally, our design has the potential for a small, low-power system where the massive components of the LiDAR are external to the small robot. We show the utility of our approach in simulation as well as hardware. We believe that this LiDAR, with its compact movable scanning stage, will enable simplified and more accurate algorithms for localization, mapping, object detection and others for microrobots.**

I. INTRODUCTION

Recently, there have been significant developments in the design of miniature robots such as robotic bees [37], crawling and walking robots [10], and small UAVs [20]. In fact, they are listed as one of the ten grand challenges in science robotics [39]. Designing such robots come with various challenges including extreme size and weight constraints on sensors, limited energy budget for computing and sensing as well as stringent limitations on the computing abilities for their functionality. A typical requirement for most robots is their ability to perceive, including both proprioceptive perception, such as robot location, as well as exteroceptive perception, such as the environment. However, micro-robots place stringent restrictions on the design of the sensors as well as onboard sensing algorithms.

Challenges for micro-robotic sensor design: The primary challenge for perception on micro-robots are the severe constraints of size, weight and power on any onboard sensing. Additionally, limited baseline for stereo sensing and limited computing and memory for onboard sensor processing make it difficult to use onboard cameras. Time-of-flight (TOF) methods, such as LiDAR, are promising but existing sensors require motorized scanners equipped with stacks of lasers and detectors that are typically heavy.

A second challenge is that the egomotion of such a robot (and, correspondingly the sensor) is quite extreme and makes any sensing challenging. For example, flapping-wing robots such as the RoboBee exhibit a high frequency rocking motion (at about 120 Hz) due to the piezo-electric actuation [9]. Environmental factors such as wind affect micro-robots to a greater extent than a larger robot. There might be aerodynamic instability due ornithopter-based shock absorption [38]. While there have been software methods to correct for such effects for cameras [3] and LiDARs [21], this is often difficult to perform in real-time onboard due to the computational and energy constraints on the robot mentioned above. It would be ideal for sensors to perform such correction in hardware without requiring onboard computing help. In this work, we propose the design of an IMU-compensated LiDAR to address this challenge.

Scanning MEMS mirrors with microrobots: Microelectromechanical (MEMS) technology provides a viable alternative for laser scanner that can minimize the weight and size of the LiDAR [31, 14, 15]. However, even with the MEMS mirror's small size and light weight, the LiDAR is still too large and heavy because of other necessary components, like the laser, photodetector, optics, the driver circuit, and the signal processing circuitry. Furthermore, to enable real-time compensated scanning, the MEMS mirror direction must be controlled for arbitrary orientations in real-time.

We solve the twin challenges of form-factor and egomotion with the following algorithmic and design contributions:

- We present a simple, effective design, Figure 1, where the LIDAR power and laser are delivered by tethers. Only the tether tip, the MEMS mirror, and photodetector will move with the micro-robot.
- We build on our prior, specially designed electrothermal MEMS mirror for this LiDAR [35]. This design enables wide non-resonant scanning angle for arbitrary orientations. It has a fast response time (5 ms), allowing high frequency egomotion compensation (up to 200 Hz).
- We show a proof-of-concept prototype combining an inertial measurement unit (IMU) with the MEMS mirror for egomotion compensation. The frequencies of the mirror modulation and IMU measurement are much higher than typical robot egomotion challenges. Our prototype IMU-based MEMS compensated scan system can perform such compensation in under 10 ms.
- We describe and geometrically characterize our sensor, showing that compensation in hardware can reduce the number of unknowns for proprioceptive and exteroceptive tasks such as Simultaneous Localization and Mapping (SLAM). In simulation, we characterize the effect of compensation delay and compensation rate to identify benefits for sensing on micro-robots.

[1,3]Dingkang Wang and Sanjeev Koppal are with the Department of Electrical and Computer Engineering; Lenworth Thomas is with the Department of Mechanical and Aerospace Engineering, University of Florida, Gainesville, FL 32603, USA noplaxochia@ufl.edu, sjkoppal@ece.ufl.edu, lenworth.thomas@ufl.edu

[2]Yuyang Chen and Karthik Dantu are with the Department of Computer Science and Engineering, University at Buffalo, Buffalo, NY 14228, USA yuyangch@buffalo.edu, kdantu@buffalo.edu

[4]Huikai Xie is with the School of Information and Electronics, Beijing Institute of Technology, Beijing, 100811, China hk.xie@ieee.org

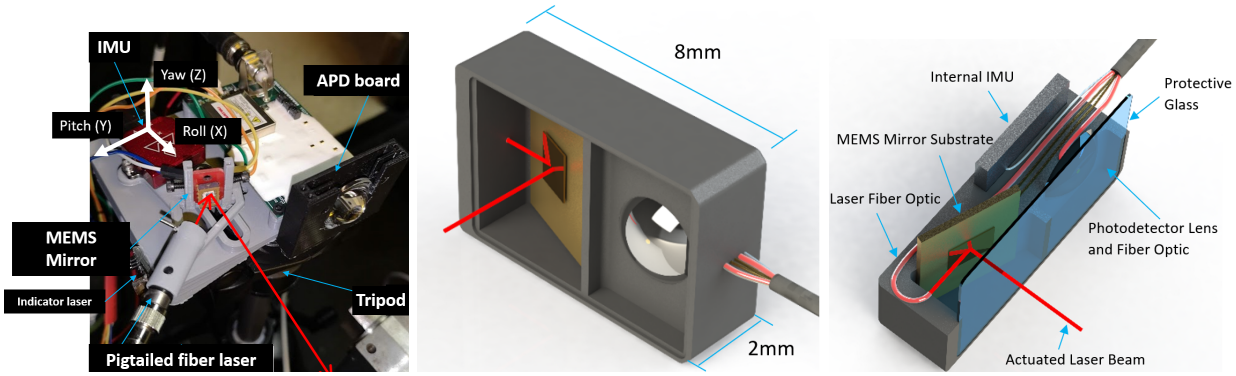

Fig. 1: Prototype motion-compensated LiDAR (left), and our envisioned design for micro-robots.

Our envisioned design for the use of such a LiDAR as well as an image of our prototype are shown in Figure 1.

II. Related Work

Small, compact LiDAR for small robotics: MEMS mirrors have been studied to build compact LiDAR systems [31, 14, 15]. For instance, Kasturi et al. demonstrated a UVA-borne LiDAR with an electrostatic MEMS mirror scanner that could fit into a small volume of 70 mm $\times$ 60 mm $\times$ 60 mm and weighed about only 50 g [14]. Kimoto et al. developed a LiDAR with an electromagnetic resonant MEMS mirror for robotic vehicles [15].

Motion compensated imaging and 3D perception: Software-based compensation for robot motion has been studied in great detail in SLAM algorithms [30] and in IMU-based compensation for camera shake [13]. These have also been used in particular for LIDAR [22] and sensing on flying systems [26]. In contrast to these approaches, we wish to compensate the sensor in hardware, during image capture.

These ideas are closer to how point-tilt-zoom cameras track dynamic objects [16, 11] and assist with background subtraction [27]. However, compared to these approaches, we can tackle egomotion of much higher frequencies, which is a unique challenge of micro-robots. We compensate signals much closer to those seen in adaptive optics and control for camera shake [1, 33, 2]. In addition, our system is on a free moving robot, rather than a fixed viewpoint.

Motorized gimbals: Comparing to motorized image stabilization systems [12], MEMS mirrors not only have smaller size and lighter weight, but their frequency response bandwidth are better than the bulky and heavy camera stabilizer. The frequency response bandwidth of most of the MEMS mirror ranges from 80 Hz to a few kHz [36, 19, 6], so the MEMS mirror response time is can be less than 10 ms or even less than 1 ms. The servo motor of the camera stabilizer has a bandwidth width less than 30 Hz because they are bulky and have heavy load [17, 24]. This results in a response time higher than 10 ms.

Motion compensation in displays and robotics: Motion-compensated MEMS mirror scanner has been applied for projection, [7], where hand-shake is an issue. In contrast, we deal with the vibration of much higher frequencies, and our approach is closest to adaptive optics for robotics. For example, [29, 28] change the zoom and focal lengths of cameras for SLAM. We compensate using small mirrors, utilizing a rich tradition of compensation in device characterization[18] and to improve SNR [8]. Compared to all the previous methods, we are the first to show IMU-based LiDAR compensation with a MEMS mirror in hardware.

Sensor reorientation in Active SLAM: There has been a lot of work in the area of perception-aware path planning. A basic assumption of this line of work is that the sensor is rigidly attached to the robot, and therefore, its field of view can be changed only by changing the pose of the robot. [4][23][5] improve SLAM accuracy by actively changing the robot trajectory to improve the field-of-view. Our sensor can simplify these works by changing the FOV in hardware without requiring additional constraints on the path planning.

III. IMU-Compensated LiDAR for Robotics

A. Basic background

A MEMS-based LIDAR scanning system consists of a laser beam reflected off a small mirror. Voltages control the mirror by physically tilting it to different angles. This allows for LIDAR depth measurements at the direction corresponding the mirror position. In the following discussion, we assume the function controlling the azimuth be $\phi(V(t))$ and the function controlling the elevation be $\theta(V(t))$, where V is the input voltage that varies with timestep t.

To characterize our sensor, we use the the structure-from-motion (SFM) framework for a LiDAR. We start with the LIDAR projection matrix $\mathbf{P}$ from the robot's rotation $\mathbf{R}$ and translation t, given the intrinsic parameters $\mathbf{K}$

$$\mathbf{P} = \mathbf{K}\ \mathbf{R}\ t. \tag{1}$$

In our scenario, the 'pixels' relate to the mirror vector orientation $(\theta(V(t)), \phi(V(t))$ on a plane at unit distance from the mirror along the z-axis. For a static scene and sensor, these 'pixel' projections $\mathbf{x}$ of LIDAR-measured 3D points $\mathbf{X}$ are trivial to obtain. However, doing so for dynamic scenes for LIDAR measurements at other robot poses is known as point-cloud alignment, and is harder. It requires recovering the unknown rotation and translation that minimize the following optimization,

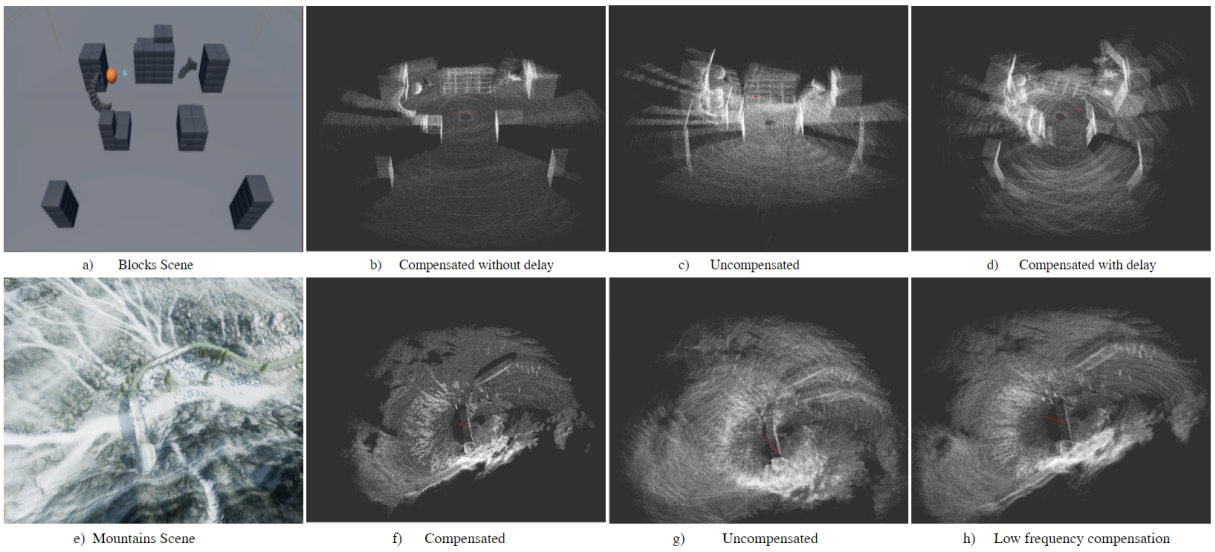

Fig. 2: (a) Representative simulation scenario - Blocks scene (b) Mapping the Blocks scene with compensation at 55Hz and no delay (c) Mapping the Blocks scene without compensation (d) Mapping the Blocks scene with compensation at 55Hz and delay of 150ms. (e) Mountains scene (f) mountains scene simulation with 55Hz compensation and 0ms delay (g) mountains scene simulation without compensation. (h) mountains scene simulation with 5Hz compensation and 0ms delay.

$$\min_{\mathbf{R},t} \|\mathbf{x} - \mathbf{PX}\|. \tag{2}$$

This optimization *usually happens in software, after LIDAR and IMU measurements*. For real systems with noise and latency, there exist modern probabilistic models that allow for smooth, high quality reconstructions and robot pose estimation [32].

Our key idea is that the MEMS mirror provides an opportunity to compensate or control two aspects of the projection matrix $\mathbf{P}$ *before capture, in hardware.*

We exploited this in our previous work [31], to control the focal length to change LIDAR zoom. More concretely, the intrinsic matrix is given by

$$\mathbf{K} = \begin{bmatrix} f_x & s & c_x \\ 0 & f_y & c_y \\ 0 & 0 & 1 \end{bmatrix} \tag{3}$$

where f_x and f_y are the focal lengths in both dimensions, (c_x, c_y) is the center of projection and s is the skew. As we previously showed [31], all these can be changed by manipulating the MEMS angles $(\theta(V(t)), \phi(V(t))$.

In this paper, we propose to control a new aspect of the SFM equation in hardware: the rotation matrix $\mathbf{R}$. The only assumption here is that the rotation of the robot happens within the field-of-view (FOV) of the system.

An onboard IMU provides instaneous angles, and therefore the known rotation matrix (and the intrinsic matrix) allow for a simplified post-capture translation estimation,

$$\min_{t} \|\mathbf{x} - \mathbf{PX}\|. \tag{4}$$

In other words, hardware compensation with MEMS mirrors simplifies the post-capture LIDAR alignment methods, allowing for lightweight and low-latency algorithms to be used on-board small, power-constrained robots. We now confirm this observation with simulated experiments.

B. Benefits of IMU-compensated LIDAR

We demonstrate the benefits of motion compensated LiDAR in simulation. Our setup is as follows - we use Airsim [25] running on Unreal Engine 4 for realistic perception and visualization. We tested two scenarios - a scene with geometric objects, called *Blocks scene* shown in Figure 2(a), and an outdoor scene with a bridge and mountains, called *Mountains scene* shown in Figure 2(e). In both scenes, the LiDAR is mounted on a prototype quadrotor UAV. It runs LOAM [40], an open-source state-of-the-art LiDAR SLAM system to map the environment and localize the UAV.

As described earlier, motion compensation can be achieved through various means such as a gimble, active compensation of a pan-tilt-zoom camera or MEMS-based hardware compensation like our system. The differences between these methods are along two dimensions - (i) latency of compensation, called *compensation delay* from now on, and (ii) number of times we can compensate in a second, called *compensation rate*. By varying these two parameters in simulation, we compare each method's performance.

In order to systematically compensate based on IMU input, we perform some pre-processing of the IMU data. To smooth out the high angular velocity body movements, an angular moving average LiDAR stabilization algorithm is implemented. This method stores the past UAV orientations in a sliding, fix length queue, and reorients the mounted LiDAR towards the average of the past orientations. This helps remove the impulsive jerky movements that may be observed by the LiDAR, akin to a low-pass filter.

In the experiment, the UAV performs three back-and-forth lateral flights between two way points. During the alternation of way points, the UAV reaches 130 $degrees/s$ in the X body

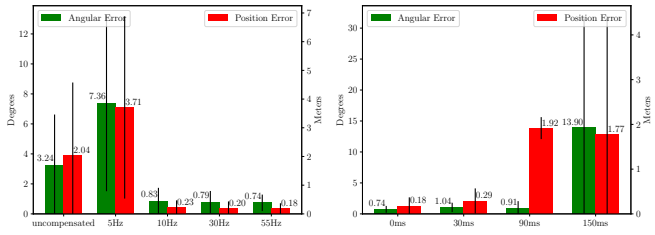

Fig. 3: UAV odometry error in the Blocks scene when (a) varying compensation rate, (b) varying compensation delay

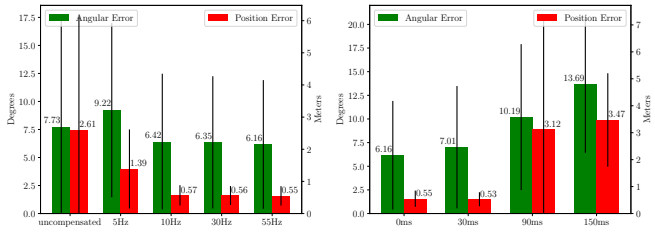

Fig. 4: UAV odometry error in the Mountains scene when (a) varying compensation rate, (b) varying compensation delay

axis. The mounted LiDAR is configured at 16 channels, 360 degree horizontal FOV, 30°vertical FOV and with 150,000 Hz sample rate, akin to commercially available LIDARs.

To quantify performance, we calculate *odometry error*, the difference between the ground truth UAV positions and those positions estimated by LOAM. Figure 3 and Figure 4 show the results from our simulations for the Blocks scene and Mountains scene respectively. We set the compensation rate to five different values - uncompensated, 5Hz, 10 Hz, 30 Hz, and 55 Hz. We set the compensation delay to five values - no delay (0 ms), 30 ms, 90 ms and 150 ms.

Both the position error and angular error are high when the compensation rate is uncompensated or 5 Hz. It is very low for 10 Hz, 30 Hz and 55 Hz. This shows that smaller rates of compensation as performed by a mechanical gimbal or a PTZ camera are far less effective than a faster compensation mechanism such as the one proposed by us. Similarly, the error in position as well as orientation is low when the compensation delay is either 0ms or 30 ms. For larger compensation delays such as 90ms and 150 ms, the error is several times that of when the compensation delay is 30 ms. This shows that as the compensation delay is higher, as it could be with software-based compensation on low-power embedded systems, it is far less effective and leads to greater error in trajectory estimation. This further argues for a system such as ours that is able to perform compensation in hardware, and therefore at a higher rate.

This proof-of-concept set of simulations encouraged us to build our proposed system.

IV. Novel LiDAR System Design

We propose a simple and effective design, shown in Fig. 5, where the MEMS mirror, IMU and photodetector are placed on a movable head. A LIDAR engine and accompanying electronics are tethered to this device, which can be light and small enough for micro-robots, as shown in Fig. 1.

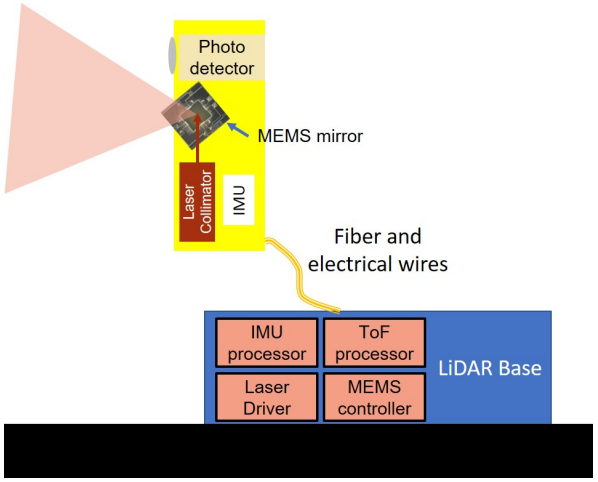

Fig. 5: The schematic of the motion compensated LiDAR with a movable LiDAR head.

A. MEMS mirror shock robustness

All the compensation effects and size advantages described so far will be nullified if the MEMS mirror cannot survive the shock, vibration and shake associate with small micro-robots. Here we analyze the robustness of the MEMS mirror device for such platforms.

Most MEMS mirrors rely on high-quality factor resonant scanning to achieve wide field-of-view (FoV), which leads to heavy ringing effects and overshoot with sudden changes of direction [19, 34]. A suitable MEMS mirror with motion-compensated scanning capability should have a wide non-resonant scanning angle and smooth and fast step responses.

We used our prior MEMS mirror fabrication [35] (Fig. 6) in our design. It has a maximum actuation voltage of 5 V and a scanning FoV of $-4.8°$ to $+5.2°$ in the horizontal axis and $-3.8°$ to $+4.3°$ in the vertical axis. The voltage to MEMS tilting angle response is approximately linear. The MEMS mirror can perform non-resonant arbitrary scanning or pointing according to the control signal. The piston resonant mode is found at f_1=1.07kHz and the tip-tilting resonant modes are at f_2 =1.63 kHz and f_3 = 1.69 kHz.

We now show expressions for the acceleration and forces generated by a MEMS mirror scan. The small-angle tip-tilt scanning stiffness k_r is

$$k_\mathrm{r} = I(2\pi f_r)^2 \tag{5}$$

where f_r is the resonant frequency of the tip-tilting modes (f_2, f_3); I is the moment of inertia of the mirror plate alone its tip-tilting axis,

$$I = \frac{1}{12} m_{\text{plate}}(t^2 + d^2) \tag{6}$$

where t is the thickness of the mirror plate, and d is the length of the mirror plate. The rotation stiffness k_r = 2.16e-6 N·m/rad. With an external angular acceleration of $\ddot{\theta}$ alone on the mirror rotation axis, the excited mirror rotation θ is

$$\theta = -\frac{I\ddot{\theta}}{k_r} = \text{-1e-8} \cdot \ddot{\theta}. \tag{7}$$

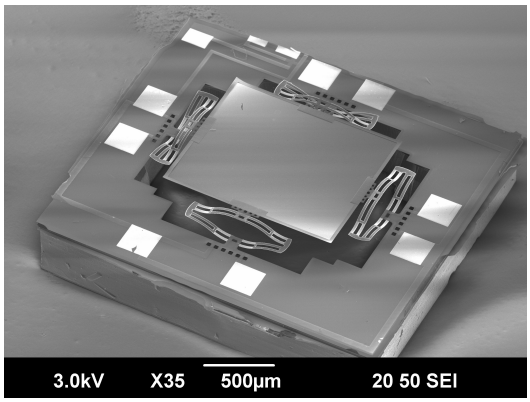

Fig. 6: An SEM image of the fabricated MEMS mirror.

The MEMS mirror is actuated by 15 kHz modulated PWM signals and has a non-resonant pointing accuracy of 0.25° in the worst case. Take the 0.25° as the maximum tolerance of the excited mirror plate rotation, the tolerable external angular acceleration is $\ddot{\theta}$ = 44000 rad/s^2. The maximum angular acceleration of a commercialized robot is usually less than 1000 rad/s^2, and the excited MEMS mirror rotation is less than 6e-4° which can be ignored. *Since this MEMS mirror has four identical actuators and the difference on the two axes alone are small, the excited MEMS mirror rotation under robot vibration can be ignored.*

We now consider robot crash scenarios. The MEMS mirror can also survive most of the extreme vibration or mechanical shock without failure. The stiffness of the MEMS mirror under shock k_{p} is:

$$k_{\text{p}} = m_{\text{plate}}(2\pi f_1)^2 \tag{8}$$

where m_{plate} is the mass of the mirror plate. Thus, the stiffness the MEMS mirror in piston motion is k_p = 3.2 N/m. The maximum allowable piston displacement of the mirror plate without failure is d_{max}= 200 μ m. The maximum tolerable acceleration in the direction perpendicular to the mirror plate is a_{max} is

$$a_{max} = \frac{k_{\text{p}} d_{\text{max}}}{m_{\text{plate}}} = 5500\text{m/s}^2. \tag{9}$$

For most commercial robots, maximum tolerable shock is under 1000 m/s^2. *So the MEMS mirror can survive most of the mechanical shock and vibration of the robot.* External vibration around the resonant frequency will excite large MEMS mirror vibration or even damage the mirror. To avoid the resonance effect, the MEMS mirror should avoid being actuated around the resonant frequency (f_1, f_2, f_3).

V. MEMS Mirror Compensation Algorithm

In the previous sections, we saw the advantages of MEMS mirror-based compensation and the feasibility for application on small robotic systems. Here we focus on the details of the simple, hardware-based rotation compensation using both IMU and MEMS mirror scanning LiDAR.

Assume the initial position of the LiDAR and the origin of the LiDAR point cloud are at the same point. At time zero, the LiDAR is at location $[lx_0 = 0, ly_0 = 0, lz_0 = 0]$ with pose $[rx_0, ry_0, rz_0]$. We combine these location and states as $L_0 = [lx_0, ly_0, lz_0, rx_0, ry_0, rz_0]$.

The MEMS mirror scanner scans the scene at different angles, given by its azimuth and elevation $[\theta_0, \phi_0]$. At each scanned angle, a LIDAR engine reflects a modulated beam and processes it to get a time-of-flight distance r_0. This measurement data $\overline{M_0} = [\theta_0, \phi_0, r_0]$ is converted to Cartesian coordinate system $\overline{P_0} = [x_0, y_0, z_0]$ in the LiDAR local coordinate. This local location $\overline{P_0}$ has a corresponding world coordinate at P_0.

Now we model the robot shake and jitter. At time t, let this shake move the LIDAR by $\Delta L_t = [\Delta lx_t, \Delta ly_t, \Delta lz_t, \Delta rx_t, \Delta ry_t, \Delta rz_t]$ according to the IMU measurement, where $L_t = L_0 + \Delta L_t$. The LiDAR needs to update the MEMS scanning direction to (θ_t, ϕ_t) so that the laser beam can still scan at the object. This is the goal of compensation, and our **contribution** here is to achieve it in hardware, for MEMS scanning LIDAR, for the first time.

The target object position $\overline{P_0}$ is transferred to $\overline{P_t}$ in the coordinate system of LiDAR-based on the LiDAR motion changes ΔL_t,

$$\overline{P_t} = R(\begin{bmatrix}\overline{P_0}\\ 0\end{bmatrix} - T), \tag{10}$$

where R is the rotation matrix, and T is the translation matrix, $R = R_x R_y R_z$, where

$$R_x = \begin{bmatrix} 1 & 0 & 0 & 0 \\ 0 & \cos(\Delta rx) & -\sin(\Delta rx) & 0 \\ 0 & \sin(\Delta rx) & \cos(\Delta rx) & 0 \\ 0 & 0 & 0 & 1 \end{bmatrix} \tag{11}$$

$$R_y = \begin{bmatrix} \cos(\Delta ry) & 0 & \sin(\Delta ry) & 0 \\ 0 & 1 & 0 & 0 \\ -\sin(\Delta ry) & 0 & \cos(\Delta ry) & 0 \\ 0 & 0 & 0 & 1 \end{bmatrix} \tag{12}$$

$$R_z = \begin{bmatrix} \cos(\Delta rz) & -\sin(\Delta rz) & 0 & 0 \\ \sin(\Delta rz) & \cos(\Delta rz) & 0 & 0 \\ 0 & 0 & 1 & 0 \\ 0 & 0 & 0 & 1 \end{bmatrix} \tag{13}$$

$$T = \begin{bmatrix} \Delta lx \\ \Delta ly \\ \Delta lz \\ 0 \end{bmatrix} \tag{14}$$

The desired MEMS mirror angle that *compensates for this motion* is (θ_t, ϕ_t), and it can be calculated as

$$\theta_t = \arccos \frac{z_t}{x_t^2 + y_t^2 + z_t^2}, \tag{15}$$

and

$$\phi_t = \arctan \frac{y_t}{x_t}. \tag{16}$$

The point clouds at different time frames can be stitched together, in software, using the world coordinates P_0 and the post-capture estimation discussed in Eq. 4.

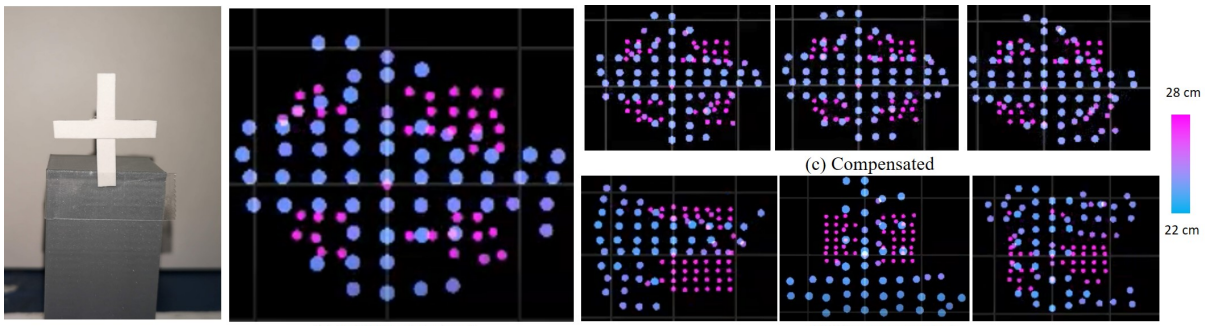

Fig. 7: (a) The target object "+" placed 22 cm from the LiDAR, along with (b), its initial point cloud scan. (c) and (d) show uncompensated vs. compensated scanning. Uncompensated shake range was $X : [-1.7°, +1.4°], Y : [-3.3°, +2.6°]$ and compensated shake range was $X : [-1.3°, +1.3°], Y : [-2.6°, +3.0°]$. (Please see supplementary video).

VI. Experiments with Hardware Prototype

Hardware specifics: Our prototype (Fig. 1) uses an avalanche photodiode module (APD, Hamamatsu C12702-04). A fiber with a length of 30 cm delivers the laser from the laser source to the scanner head. The laser is collimated and reflected by the MEMS mirror. The X-axis of the IMU (VectorNav, VN-100) is parallel to the neutral scanning direction of the MEMS mirror. The accuracies of the IMU measurements are 0.5° in the pitch and roll directions and 2° in the yaw direction, respectively. The scanner head sits on a tripod so that it can be rotated in the yaw and pitch directions. In the LiDAR base, an Arduino microcontroller is used to process the ToF signals, sample the IMU signals and control the MEMS mirror scanning direction. The data are sent to a PC for post-processing and visualization.

Since we focus on proximity detection for small robots (for landing or docking), our maximum detection distance is 35 cm with a 80% albedo object and the minimal resolvable distance is 1 cm. A more advanced LIDAR could be swapped in, and the rest of our contributions would still remain.

The maximum ToF measurement rate is 200 points/sec, and the IMU is sampled at every ToF measurement. According to the compensation algorithm described in the previous section, the MEMS mirror scanning direction is updated with every IMU measurement. We now describe our experiments. Please see the accompanying video for better viewing.

Compensation experiments with zero translation: We place the prototype on a tripod so it can be rotated freely, as shown in Figure 1. A paper-cut figure is placed 22cm away from the LiDAR and at the center of the FoV, as shown in Figure 7a. The MEMS mirror performs a raster scanning pattern with an initial FoV of $-2°$ $+2°$ in both axes to leave the room for compensation. Each frame has 10 by 10 pixels, and the frame refresh rate is 2 fps. To mimic robot vibration, the tripod is rotated randomly in the directions of yaw (Z-axis) and pitch (Y-axis), and the point clouds are shown in Figures 7c. Despite the motion of the LiDAR head, the point clouds are quite stable. The differences among all of the point clouds are generally less than 1 pixel in either axis, caused by measurement noise. Even with a continuous rotation with a frequency of 1.5 Hz, the point cloud still remains stable, as shown in the 3rd figure in Figure 7c.

Figures 7d shows the point clouds without compensated scanning, where the relative positions of the target object in the point clouds keep changing. The target object may come out of the MEMS scanning FoV without compensation. With a continuous rotation of 1.5 Hz in the Y-axis, the same structure may appear in multiple positions in the same frame of the point cloud, as shown in the 3rd figure of Figure 7d. In order to creating the mapping point cloud from stitching the point cloud from different view, the MEMS mirror scanning direction should compensated the disturbance in motion.

Compensation experiments with translation: Here, we performed point-cloud stitching as that sensor moves along an object. The target scanning area is along the horizontal paper-cut figure shown in the highlighted area in the Figure 8 (a). The blue line is an example of the true motion with disturbance only existing in the vertical direction. As the LiDAR rotates from in the horizontal direction from left to right, it is expected to collect the best point cloud covering the highlight area of the object only. The result of compensated scanning and uncompensated scanning are shown in Figures 8 (b) and (c) on the right side, with their measured motions on the left side.

VII. Conclusions and Limitations

We believe that ours is the first IMU-compensated MEMS mirror scanning LIDAR. Through simulation and a proof-of-concept implementation we realize our design shown in Fig 1. This design separates the sensor into two components - a small, lighter part that can be mounted on the robot connected to the heavier part using a tether. Although removing the tether restriction is left to future work, we believe that our design is capable of advancing sensing in microrobots significantly, and will help our community in designing microrobots in the future.

References

[1] Riccardo Antonello et al. "IMU-aided image stabilization and tracking in a HSM-driven camera positioning

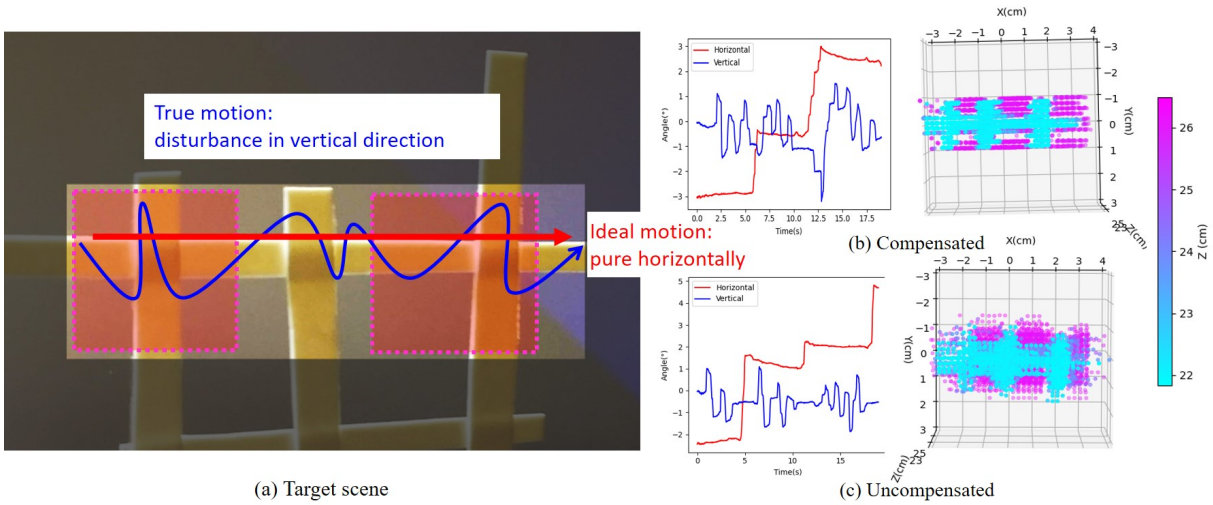

Fig. 8: Compensated point cloud stitching and experiment and its results. (a) The target scene placed at 22 cm from the LiDAR. The red line is the ideal motion, the blue line qualitatively depicts the type of experiment we performed, with vertical disturbances only. The graphs show the actual, measured disturbances. (b) With compensated scanning, the recorded motion and the generated point cloud show sharper depth edges than that with (c) with uncompensated scanning.

unit". In: *2013 IEEE International Symposium on Industrial Electronics*. IEEE. 2013, pp. 1–7.

[2] Moshe Ben-Ezra, Assaf Zomet, and Shree K Nayar. "Jitter camera: High resolution video from a low resolution detector". In: *Proceedings of the 2004 IEEE Computer Society Conference on Computer Vision and Pattern Recognition, 2004. CVPR 2004.* Vol. 2. IEEE. 2004, pp. II–II.

[3] Chao-Ho Chen et al. "Real-time video stabilization based on motion compensation". In: *2009 Fourth International Conference on Innovative Computing, Information and Control (ICICIC)*. IEEE. 2009, pp. 1495–1498.

[4] Gabriele Costante et al. "Perception-aware Path Planning". In: *IEEE Transactions on Robotics* (2016), Epub–ahead.

[5] Xinke Deng et al. "Feature-constrained active visual SLAM for mobile robot navigation". In: *2018 IEEE International Conference on Robotics and Automation (ICRA)*. IEEE. 2018, pp. 7233–7238.

[6] F Filhol et al. "Resonant micro-mirror excited by a thin-film piezoelectric actuator for fast optical beam scanning". In: *Sensors and Actuators A: Physical* 123 (2005), pp. 483–489.

[7] Heinrich Grüger et al. "3.1: MOEMS Laser Projector for Handheld Devices Featuring Motion Compensation". In: *SID Symposium Digest of Technical Papers*. Vol. 38. 1. Wiley Online Library. 2007, pp. 1–3.

[8] Tomohiko Hayakawa et al. "Gain-compensated sinusoidal scanning of a galvanometer mirror in proportional-integral-differential control using the pre-emphasis technique for motion-blur compensation". In: *Applied Optics* 55.21 (2016), pp. 5640–5646.

[9] E Farrell Helbling, Sawyer B Fuller, and Robert J Wood. "Pitch and yaw control of a robotic insect using an onboard magnetometer". In: *2014 IEEE international conference on robotics and automation (ICRA)*. IEEE. 2014, pp. 5516–5522.

[10] Katie Lynn Hoffman. "Design and locomotion studies of a miniature centipede-inspired robot". PhD thesis. 2013.

[11] Stefan Hrabar, Peter Corke, and Volker Hilsenstein. "PTZ camera pose estimation by tracking a 3D target". In: *2011 IEEE International Conference on Robotics and Automation*. IEEE. 2011, pp. 240–247.

[12] Ruting Jia et al. "System performance of an inertially stabilized gimbal platform with friction, resonance, and vibration effects". In: *Journal of Nonlinear Dynamics* 2017 (2017).

[13] Alexandre Karpenko et al. "Digital video stabilization and rolling shutter correction using gyroscopes". In: *CSTR* 1.2011 (2011), p. 2.

[14] Abhishek Kasturi et al. "UAV-borne lidar with MEMS mirror-based scanning capability". In: *Laser Radar Technology and Applications XXI*. Vol. 9832. International Society for Optics and Photonics. 2016, p. 98320M.

[15] Katsumi Kimoto et al. "Development of small size 3D LIDAR". In: *2014 IEEE International Conference on Robotics and Automation (ICRA)*. IEEE. 2014, pp. 4620–4626.

[16] GEN LI et al. "Tracking moving objects by using a pan-tilt-zoom camera". In: *ITC-CSCC: International Technical Conference on Circuits Systems, Computers and Communications*. 2009, pp. 1012–1015.

[17] Quanchao Li et al. "Nonorthogonal Aerial Optoelectronic Platform Based on Triaxial and Control Method Designed for Image Sensors". In: *Sensors* 20.1 (2020), p. 10.

[18] Ievgeniia Maksymova et al. “Detection and Compensation of Periodic Jitters of Oscillating MEMS Mirrors used in Automotive Driving Assistance Systems”. In: *2019 IEEE Sensors Applications Symposium (SAS)*. IEEE. 2019, pp. 1–5.

[19] Veljko Milanović et al. “Closed-loop control of gimbal-less MEMS mirrors for increased bandwidth in LiDAR applications”. In: *Laser Radar Technology and Applications XXII*. Vol. 10191. International Society for Optics and Photonics. 2017, 101910N.

[20] Yash Mulgaonkar, Gareth Cross, and Vijay Kumar. “Design of small, safe and robust quadrotor swarms”. In: *2015 IEEE international conference on robotics and automation (ICRA)*. IEEE. 2015, pp. 2208–2215.

[21] Tao Peng and Satyandra K Gupta. “Model and algorithms for point cloud construction using digital projection patterns”. In: (2007).

[22] Ethan Phelps and Charles A Primmerman. “Blind Compensation of Angle Jitter for Satellite-Based Ground-Imaging Lidar”. In: *IEEE Transactions on Geoscience and Remote Sensing* 58.2 (2019), pp. 1436–1449.

[23] Seyed Abbas Sadat et al. “Feature-rich path planning for robust navigation of MAVs with mono-SLAM”. In: *2014 IEEE International Conference on Robotics and Automation (ICRA)*. IEEE. 2014, pp. 3870–3875.

[24] Artur Sagitov and Yuri Gerasimov. “Towards DJI phantom 4 realistic simulation with gimbal and RC controller in ROS/Gazebo environment”. In: *2017 10th International Conference on Developments in eSystems Engineering (DeSE)*. IEEE. 2017, pp. 262–266.

[25] Shital Shah et al. “Airsim: High-fidelity visual and physical simulation for autonomous vehicles”. In: *Field and service robotics*. Springer. 2018, pp. 621–635.

[26] Takumi Shinohara and Toru Namerikawa. “SLAM for a small UAV with compensation for unordinary observations and convergence analysis”. In: *2016 55th Annual Conference of the Society of Instrument and Control Engineers of Japan (SICE)*. IEEE. 2016, pp. 1252–1257.

[27] Jae Kyu Suhr et al. “Background compensation for pan-tilt-zoom cameras using 1-D feature matching and outlier rejection”. In: *IEEE transactions on circuits and systems for video technology* 21.3 (2010), pp. 371–377.

[28] Takafumi Taketomi and Janne Heikkila. “Focal length change compensation for monocular slam”. In: *2015 IEEE International Conference on Image Processing (ICIP)*. IEEE. 2015, pp. 4982–4986.

[29] Takafumi Taketomi and Janne Heikkilä. “Zoom factor compensation for monocular SLAM”. In: *2015 IEEE Virtual Reality (VR)*. IEEE. 2015, pp. 293–294.

[30] Takafumi Taketomi, Hideaki Uchiyama, and Sei Ikeda. “Visual SLAM algorithms: a survey from 2010 to 2016”. In: *IPSJ Transactions on Computer Vision and Applications* 9.1 (2017), p. 16.

[31] Zaid Tasneem et al. “Adaptive fovea for scanning depth sensors”. In: *The International Journal of Robotics Research* (2020), p. 0278364920920931.

[32] Sebastian Thrun. “Probabilistic robotics”. In: *Communications of the ACM* 45.3 (2002), pp. 52–57.

[33] Robert K Tyson. “Performance assessment of MEMS adaptive optics in tactical airborne systems”. In: *Adaptive Optics Systems and Technology*. Vol. 3762. International Society for Optics and Photonics. 1999, pp. 91–100.

[34] Dingkang Wang, Connor Watkins, and Huikai Xie. “MEMS Mirrors for LiDAR: A review”. In: *Micromachines* 11.5 (2020), p. 456.

[35] Dingkang Wang et al. “A low-voltage, low-current, digital-driven MEMS mirror for low-power LiDAR”. In: *IEEE Sensors Letters* 4.8 (2020), pp. 1–4.

[36] Dingkang Wang et al. “An ultra-fast electrothermal micromirror with bimorph actuators made of copper/tungsten”. In: *2017 International Conference on Optical MEMS and Nanophotonics (OMN)*. IEEE. 2017, pp. 1–2.

[37] Robert Wood, Radhika Nagpal, and Gu-Yeon Wei. “flight of the robobees”. In: *Scientific American* 308.3 (2013), pp. 60–65. ISSN: 00368733, 19467087. URL: http://www.jstor.org/stable/26018027.

[38] Dong Xue et al. “Computational simulation and free flight validation of body vibration of flapping-wing MAV in forward flight”. In: *Aerospace Science and Technology* 95 (2019), p. 105491.

[39] Guang-Zhong Yang et al. “The grand challenges of Science Robotics”. In: *Science robotics* 3.14 (2018), eaar7650.

[40] Ji Zhang and Sanjiv Singh. “LOAM: Lidar Odometry and Mapping in Real-time.” In: *Robotics: Science and Systems*. Vol. 2. 9. 2014.